



Universiteit
Leiden
The Netherlands

Phenotypic screening with 3D cell-based assays

Booij, T.H.

Citation

Booij, T. H. (2017, December 20). *Phenotypic screening with 3D cell-based assays*. Retrieved from <https://hdl.handle.net/1887/59503>

Version: Not Applicable (or Unknown)

License: [Licence agreement concerning inclusion of doctoral thesis in the Institutional Repository of the University of Leiden](#)

Downloaded from: <https://hdl.handle.net/1887/59503>

Note: To cite this publication please use the final published version (if applicable).

Cover Page



Universiteit Leiden



The following handle holds various files of this Leiden University dissertation:
<http://hdl.handle.net/1887/59503>

Author: Booi, T.H.

Title: Phenotypic screening with 3D cell-based assays

Issue Date: 2017-12-20

chapter 3

Development of a 3D tissue culture-based high-content screening platform that uses phenotypic profiling to discriminate selective inhibitors of receptor tyrosine kinases

Tijmen H. Booij^{1#}; Maarten J.D. Klop^{2#}; Kuan Yan², Csaba Szántai-Kis³, Balint Szokol³, Laszlo Orfi^{3,4}, Bob van de Water¹; Gyorgy Keri^{3,5}, Leo S. Price^{1,2}

- 1 Division of Toxicology, Leiden Academic Centre for Drug Research, Leiden University, Leiden The Netherlands.
 - 2 Ocello B.V., Leiden, The Netherlands.
 - 3 Vichem Chemie Research Ltd., 1022 Budapest, Hungary
 - 4 Department of Pharmaceutical Chemistry, Semmelweis University, 1085 Budapest, Hungary
 - 5 MTA-SE Pathobiochemistry Research Group, Department of Medical Chemistry, Semmelweis University, 1085 Budapest, Hungary
- # Authors contributed equally to this work.

Based on: Booij TH, Klop MJ, Yan K, Szantai-Kis C, Szokol B, Orfi L, van de Water B, Keri G, Price LS: Development of a 3D Tissue Culture-Based High-Content Screening Platform That Uses Phenotypic Profiling to Discriminate Selective Inhibitors of Receptor Tyrosine Kinases. *J Biomol Screen*, 2016

Abstract

3D tissue cultures provide a more physiologically relevant context for the screening of compounds, compared to 2D cell cultures. Cells cultured in 3D hydrogels also show complex phenotypes, increasing the scope for phenotypic profiling.

Here we describe a high-content screening platform that uses invasive human prostate cancer cells cultured in 3D in standard 384-well assay plates to study the activity of potential therapeutic small molecules and antibody biologics. Image analysis tools were developed to process 3D image data to measure over 800 phenotypic parameters. Multi-parametric analysis was used to evaluate the effect of compounds on tissue morphology.

We applied this screening platform to measure the activity and selectivity of inhibitors of the c-Met and EGF receptor (EGFR) tyrosine kinases in 3D cultured prostate carcinoma cells. c-Met and EGFR activity was quantified based on the phenotypic profiles induced by their respective ligands, HGF and EGF. The screening method was applied to a novel collection of 80 putative inhibitors of c-Met and EGFR. Compounds were identified that induced phenotypic profiles indicative of selective inhibition of either c-Met, EGFR or bispecific inhibition of both targets.

In conclusion, we describe a fully scalable high-content screening platform that uses phenotypic profiling to discriminate selective and non-selective (off-target) inhibitors in a physiologically relevant 3D cell culture setting.

Introduction

While offering many practical advantages for cell based screening, cells grown on tissue culture plastic lack normal cell-cell and cell-matrix interactions, resulting in deregulated growth, dedifferentiation, disruption of other processes and a poor simulation of the *in vivo* (patho-)physiology.¹ 3D cell culture methods have been developed that enable a more *in vivo* like tissue architecture and are therefore expected to represent a more physiologically relevant context for the evaluation of bioactive molecules.²⁻⁴ Although gaining in popularity for small-scale analyses, 3D cultures have yet to be widely adopted for screening. A number of factors account for this, although high throughput 3D imaging and the analysis of large and complex image data sets can represent the most significant barrier to the implementation of high content 3D culture based screening.⁵ As a result, where 3D assays are used for screening, the most common end-point measurements tend to be biochemical determinations of cell viability, with the loss of potentially valuable phenotypic information.

Cells cultured in extracellular matrix (ECM) -containing hydrogels can generate complex multicellular tissues, supporting a higher level of tissue organisation, such as formation of ductal structures by epithelial cells and complex networks of invasive tumour cells.⁶⁻¹⁰ These features may be relevant to the pathology of the disease being studied and offer a context for screening for therapeutic molecules. Complex phenotypes can also be exploited for compound profiling, allowing compounds that affect different targets and therefore induce different phenotypes to be discriminated, potentially providing additional information on the biological effects of compounds that cannot be obtained from single end point measurements.

In many cultured cells, activation of receptor tyrosine kinases results in increased proliferation and motility.¹¹ Cell motility has previously been used as a readout for high throughput small molecule and siRNA screens for inhibitors of c-Met signalling.¹²⁻¹⁴ In 3D culture, activation of c-Met can result in invasion of tumour cells into the surrounding micro-environment,¹⁵ a process which closely resembles the *in vivo* pathophysiology. Similarly, activation of the EGF receptor is known to induce EMT and invasion in various cancer types.¹⁶⁻¹⁷ As expected, selective inhibition of the receptor tyrosine kinases inhibits the ligand induced effects. However, compounds that inhibit multiple targets or are toxic may also inhibit ligand-induced effects. Here, we describe a 384-well screening assay that uses automated high content analysis and profiling of 3D cultures of invasive prostate cancer tumour cells to identify selective inhibitors of the c-Met and EGFR receptor tyrosine kinases.

MATERIALS AND METHODS

Cell lines

The human prostate adenocarcinoma cell line PC-3 was cultured in DMEM-F12 (Ham's) growth medium (Gibco™ Fisher Scientific, Landsmeer, Netherlands), supplemented with 10% FBS (Gibco™ Fisher Scientific, Landsmeer, Netherlands), 1mM sodium

pyruvate (Gibco™ Fisher Scientific, Landsmeer), 1.5g/L NaHCO₃ (Merck, Schiphol-Rijk, Netherlands), 0.1mM non-essential amino acids (Gibco™ Fisher Scientific, Landsmeer, Netherlands) and 50µg/mL gentamycin (Sigma Aldrich, Zwijndrecht, Netherlands). PC-3 cells were grown in 175cm² tissue culture flasks (Corning, Amsterdam, Netherlands) in culture medium as described above. Before reaching maximal density, cells were washed with 1x PBS (Sigma Aldrich, Zwijndrecht, Netherlands) and trypsinized with 1x Trypsin (Gibco™ Fisher Scientific, Landsmeer, Netherlands). Subsequently, medium was added and cells were pelleted by centrifugation and resuspended in FBS with 10% DMSO (Biosolve B.V., Netherlands) and stored in aliquots at -150°C.

3D invasion assay

PC-3 cells were cultured in 384-well plates (Greiner Bio-One B.V., Alphen aan den Rijn, Netherlands) in 60%v/v growth factor-reduced Matrigel (>9mg/mL) (Corning, Amsterdam, Netherlands) which supported spheroid formation of the highly transformed PC-3 cells and invasion upon addition of motogenic cytokines. To generate gels, thawed cells were mixed with culture medium and growth factor-reduced Matrigel. 14.5µL of cell-gel mix was added to each well of a 384-well plate using a CyBi Selma 96/60 robotic liquid handler (Analytik Jena AG, Jena, Germany), at a final cell density of 2000 cells per well. After polymerization at 37°C for 30 minutes, DMEM-F12 (Ham's) growth medium containing growth factors (HGF or EGF) and compounds were added to the gel. The plate(s) were subsequently covered with a gas permeable adhesive membrane (Thermo Scientific, Zwijndrecht, Netherlands). Compound exposures were performed for 96 hours, after which gels were fixed with 3% formaldehyde (Sigma Aldrich, Zwijndrecht, Netherlands), permeabilised with 0.2% Triton-X100 (Sigma Aldrich, Zwijndrecht, Netherlands) and stained with 0.25µM rhodamine-phalloidin (Sigma Aldrich, Zwijndrecht, Netherlands) and 0.1% Hoechst 33258 (Sigma Aldrich, Zwijndrecht, Netherlands) in PBS at 4°C for 16 hours. After staining, plates were washed in PBS and covered with a Greiner SilverSeal (Greiner Bio-One B.V., Alphen aan den Rijn, Netherlands).

Compounds

Anti c-Met and non-targeting control Fab antibodies were generously provided by Merus Biopharmaceuticals B.V. (Utrecht, The Netherlands). c-Met inhibitor ArQ-197 (Tivantinib) was synthesized by Janssen Pharmaceutica NV (Beerse, Belgium), following the synthesis method published from ArQule, and subsequently sent to the authors as a gift from Souichi Ogata (Janssen Oncology R&D). Results were confirmed using a second source of ArQ-197 (SelleckChem/Bio-Connect B.V. Huissen, Netherlands). EGFR inhibitor AG1478 was obtained from Santa Cruz (SC-200613, Bio-Connect B.V. Huissen, Netherlands). PHA-665752 was a gift from Pfizer Inc. A collection of 80 compounds selected to inhibit both EGFR and/or c-Met was generated by Vichem Chemie, Budapest, Hungary (supplemental table 1).

Imaging

A BD Pathway 855 automated inverted fluorescence microscope (BD Biosciences)

was used for automated imaging of 384-well plates (wide-field epifluorescence). This microscope was used to image both Hoechst 33258 and rhodamine-phalloidin staining, using a 4x Olympus objective, at focal planes spaced at intervals of 50 μ m throughout the gel using Attovision software accompanying the microscope. The gel was imaged through its entire depth (z-axis), requiring 25 images per well. Each image captured approximately 75% of the area of the well.

Data Analysis

Ominer image analysis software (OcellO, Leiden, Netherlands) and KNIME (<https://www.knime.org>) were used to extract in-focus information from the Z-stacks generated by the BD Pathway 855 for both Hoechst 33258 (nuclei) and rhodamine-phalloidin (F-actin) using maximum-intensity projections.¹⁸ For image processing, a monochrome mask was created for both channels to define the regions of interest (ROI's). The in-focus images were used to quantify staining intensities and a set of Hu moments and Gabor wavelet based features describing image intensity and texture. The Hoechst 33258-derived monochrome mask was used to determine number and area of nuclei and tumouroids. Additionally, a detailed set of parameters was calculated to describe the shape of the rhodamine-phalloidin (F-actin) stained objects.¹⁸ First, for principal components analysis, data were Z-score normalized to the negative control treatment median to account for plate-to-plate differences. The features derived from the image analysis and quantification steps were ranked based on their ability to distinguish positive and negative controls (Z-prime) and the features that showed greatest separation between control groups were retained ($Z' > 1.0$). The median of treatment quadruplicates was used for a principal component analysis (PCA) that combined correlated features into (uncorrelated) principal components. This model was applied to all wells and summarized ~95% of all variation into principal components. The distance between treatment and control groups was quantified as a Z-score in principal component 0 (PC0), which retained 60% of the variation of the data set. 2-dimensional density estimations and linear discriminant analysis (LDA) were performed using the MASS package (<http://www.stats.ox.ac.uk/pub/MASS4/>)¹⁹ for R-studio 0.99.878 (<https://www.rstudio.com/products/rstudio2/>) with R 3.2.3 (<https://www.r-project.org/>). PCA was calculated in KNIME and principal component plots were generated using ggplot2 (<http://ggplot2.org/>)²⁰ with the scatterplot3D package for R-Studio 0.99878 (<https://cran.r-project.org/web/packages/scatterplot3d/index.html>).²¹ Other charts were generated using Graphpad Prism 6 software (<http://www.graphpad.com/scientific-software/prism/>). Results are displayed as mean \pm standard deviation unless otherwise stated.

Western blot detection of receptor activation

Phosphorylation status of c-Met and EGFR in response to 20ng/mL HGF or 20ng/mL EGF was evaluated by Western blot. Briefly, 10⁵ PC-3 cells were grown per well in 12 well plates. After 24 hours, growth medium was replaced with starvation medium (without serum and antibiotics) containing test compounds. After 24 hours of compound exposure, growth factors (20ng/mL HGF/EGF) were added for 10 minutes. Protein was

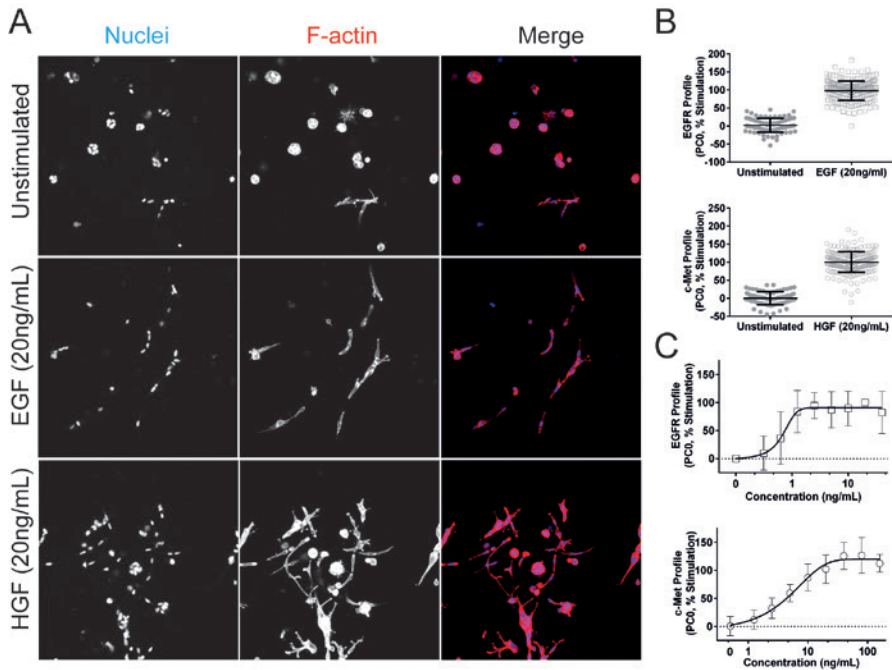


FIGURE 1 Receptor activation induces a quantifiable change in phenotype. **A)** Typical images of unstimulated, HGF- and EGF-stimulated PC-3 cells taken using a Nikon TI Eclipse confocal microscope. Receptor activation induced a change in phenotype characterized by invasion into the surrounding matrix. F-actin stained red, nuclei stained blue. **B)** Phenotypic shift induced by HGF and EGF visualized using supervised (unstimulated-stimulated) principal components analysis (PCA). PCo was scaled between 0% (unstimulated) and 100% (stimulated). Individual data points shown, as well as mean and standard deviations **C)** EGF and HGF cause a dose-dependent change in phenotype. Phenotypic change is derived from PCo and scaled to % response as shown in B. Results are shown as means with standard deviation.

isolated using RIPA lysis buffer (1%w/w deoxycholate, 50mM Tris pH7.5, 0.15M NaCl, 0.1% SDS, 1% NP-40, 2mM EDTA, 1% protease inhibitor cocktail (Sigma Aldrich, Zwijndrecht, Netherlands)) and quantified using the standard BCA method according to manufacturer's instructions (Thermo Scientific, Zwijndrecht, Netherlands). Western blot analysis was performed according to standard protocol using phospho-c-Met (Tyr1234/1235) antibody (Cell Signaling, Cat#3077P) diluted 1:1000 in 5%BSA in TBS-T or phospho-EGFR (Tyr1173) (Cell Signaling, Cat#4407) 1:1000 in 5% BSA in TBS-T. Phospho-c-Met and Phospho-EGFR antibodies were detected using HRP conjugated anti-rabbit IgG secondary antibody (Jackson, 111-035-003) and ECL Plus reagent (GE Healthcare Life Sciences, Eindhoven, The Netherlands, Cat#RPN2132). Detection of antibody was performed using a LAS4000 scanner (GE Healthcare Life Sciences,

Eindhoven, The Netherlands). Tubulin loading control was detected using an anti-Tubulin antibody (Sigma-Aldrich, Zwijndrecht, Netherlands #T-9026) diluted 1:1000 in 5%BSA in TBS-T and an anti-mouse Alexa 647-linked IgG (JacksonImmunoResearch, Suffolk, UK #115-605-006). The Alexa 647 signal was detected directly using the LAS4000.

In vitro kinase activity measurement

EGFR enzyme activity was assayed in 384 microtiter plates (Corning 3676) at 3 compound concentrations, in a total volume of 10 μ L by the Transcreener ADP2 FP method (BellBrook Labs). Assay buffer contained 20mM HEPES pH7.5, 1mM DTT, 10mM MgCl₂, 2mM MnCl₂, 0.01%v/v NP40. The final EGFR concentration was 7nM. Poly Glu-Tyr (4:1) / Poly Glu-Tyr (4:1) was used as substrate at final concentration of 0.01mg/mL. The final ATP concentration was at 7.52 μ M. The enzyme reaction was incubated for 60 minutes and stopped by addition of 10 μ L ADP detection mixture (1x). Measurements were performed on a Tecan Infinite M1000Pro reader. c-Met enzyme activity was assayed in 384 microtiter plates (Corning 3676) at 3 compound concentrations, in total volume of 10 μ L by the Transcreener ADP2 FP method (BellBrook Labs). Assay buffer contained 20mM HEPES pH7.5, 1mM DTT, 3mM MgCl₂, 3mM MnCl₂, 0.01%v/v Tween20. The final c-Met concentration was 8nM. Poly Ala-Glu-Lys-Tyr (6:2:5:1) was used as substrate at final concentration of 0.25mg/ml. The final ATP concentration was at 9.6 μ M. The enzyme reaction was incubated for 60 minutes and stopped by addition of 10 μ L ADP detection mixture (1x). Measurements were performed using a Tecan Infinite M1000Pro reader.

RESULTS

Quantification of complex phenotypic changes of prostate cancer cells cultured in 3D in 384 well microplates.

We developed a 3D cell culture screening method for tumour cell invasion driven by c-Met and EGFR. PC-3 cells were cultured in extracellular matrix (ECM) protein-rich hydrogels in 384-well plates in the presence or absence of c-Met/EGFR agonists and antagonists. After fixation and staining with rhodamine-phalloidin to reveal the structure of prostate cancer tumouroids and Hoechst 33258 to label nuclei, gels were imaged in two fluorescence channels using a BD Pathway 855, collecting paired stacks of xy images throughout the z-plane for each well. In-focus information from each image was extracted and a single xy image projection was generated (supplemental figure 1).

In the absence of added c-Met or EGFR agonists, PC₃ cells developed into spheroids over a period of 4 days (figure 1A, upper panel). Treatment with the c-Met ligand (HGF) or the EGFR ligand (EGF), induced a highly invasive phenotype (figure 1A, middle and lower panels). To quantify these phenotypic changes in detail, Ominer and KNIME software were used to identify and quantify different morphological features from the 2D projections of the cytoskeleton and nuclei-derived image stacks. To do this, a collection of different image analysis algorithms was applied to derive measurements of the shape and fluorescence intensity of individual tumouroids, and wavelets, Hu and

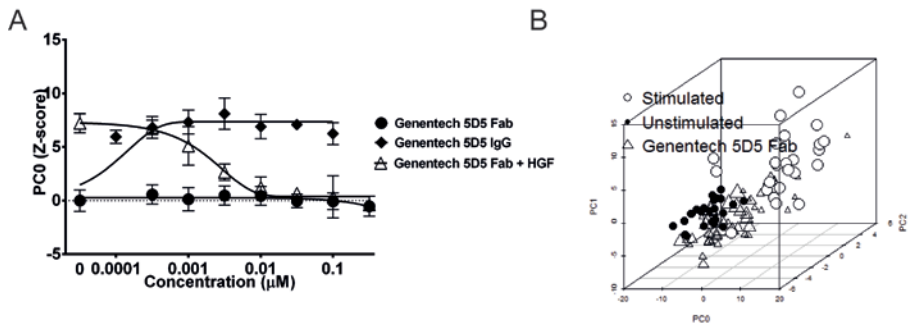


FIGURE 2 c-Met-dependent phenotypic changes. A) Inhibition of HGF-induced invasion in 3D-cultured PC-3 cells by function blocking c-Met Fab antibody 5D5 (Genentech), and stimulation of invasion by the crosslinking and activating bivalent IgG isoform. PCA trained on unstimulated and stimulated control, PC₀ shown and scaled as Z-score to unstimulated control. Results are shown as means of quadruplicate wells and standard deviations. **B)** 5D5 Fab (triangles) causes a shift in phenotype from stimulated (empty circles) back to unstimulated control (filled circles). Point size of markers for Fab treatment increases with concentration (7 concentrations, range 0.316-316nM). Individual datapoints are shown as a 3D scatterplot with PC₀, PC₁ and PC₂.

Zernike moments as previously described.¹⁸ Supervised principal components analysis (PCA) was used to reduce measurements from approximately 800 phenotypic parameters to principal components (PC). EGF-treated and untreated PC3 cells were used to train a profile to represent active and inactive EGFR inhibitors, respectively, which was subsequently scaled to %-stimulation. Similarly, a separate supervised analysis was performed which was trained with HGF-treated and untreated cells to separate phenotypes representing active c-Met from unstimulated control phenotypes. The primary principal component (PC₀) was plotted for both EGF- and HGF-induced phenotypic changes in order to visualise the responses (figure 1B). Both HGF and EGF induced phenotypes of PC-3-derived tumouroids could be clearly discriminated from untreated tissues. Many of the phenotypic features separating HGF- and EGF- induced changes in phenotype from unstimulated controls describe shape, circularity and intensity. The distance in phenotypic space along PC₀ to the unstimulated controls was presented graphically as a function of EGF or HGF concentration (figure 1C).

Phenotypic profiling can be used to quantify c-Met activation and inactivation.

To test whether HGF-induced phenotypes could report c-Met activation, HGF was added in the presence of the c-Met function blocking Fab antibody, Genentech 5D5 Fab (Genentech). 5D5 antibody effectively inhibited the HGF-induced response (PC₀, figure 2A), resulting in phenotypes that projected in a similar location to unstimulated controls in phenotypic space (represented by three principal components), with an inhibition that was dose-dependent (figure 2A and 2B). The c-Met inhibitory antibody had no

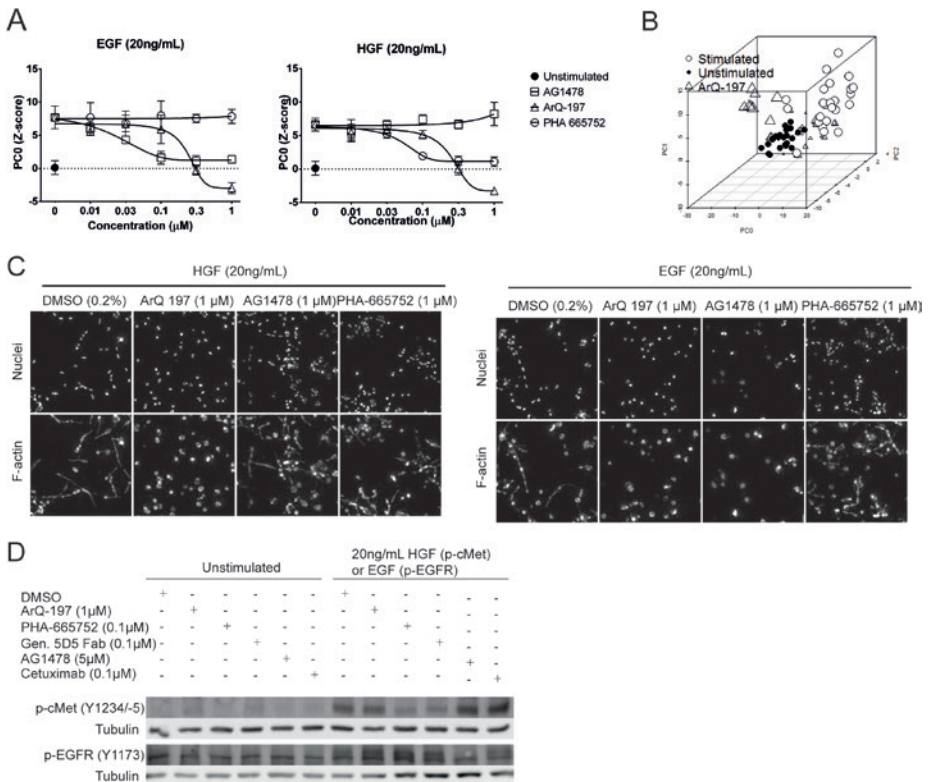


FIGURE 3 Discriminating on-target effects from off-target effects. **A)** HGF- (left panel) and EGF-induced (right panel) phenotypes can be inhibited by small molecules targeting c-Met and EGFR, respectively. Responses are shown as PCo, z-score normalized to unstimulated. Values shown as means of quadruplicate wells with standard deviation. **B)** PCA plot identifies novel phenotype introduced by ArQ-197 (triangles) at high doses. Individual data points are shown as a 3D scatterplot with PCo, PC1 and PC2. Empty circles, stimulated controls; filled circles, unstimulated controls. **C)** Representative images showing HGF and EGF induced invasion and inhibition by small molecules. Maximum intensity projections of both image channels shown. **D)** Western blot of c-Met and EGFR phosphorylation in 2D-cultured PC-3 cells exposed to EGF or HGF and inhibitors.

quantifiable effect on the PC-3 phenotype in the absence of HGF (figure 2A). In contrast, treatment of PC-3 cells with a c-Met activating antibody, the bivalent IgG form of 5D5, which crosslinks c-Met, induced a phenotype which was indistinguishable from that induced by HGF. Together these results confirm the c-Met dependency of the HGF-induced phenotype and demonstrate that principal components can be used to quantify HGF-induced phenotypic changes correlating with c-Met activation and inhibition.

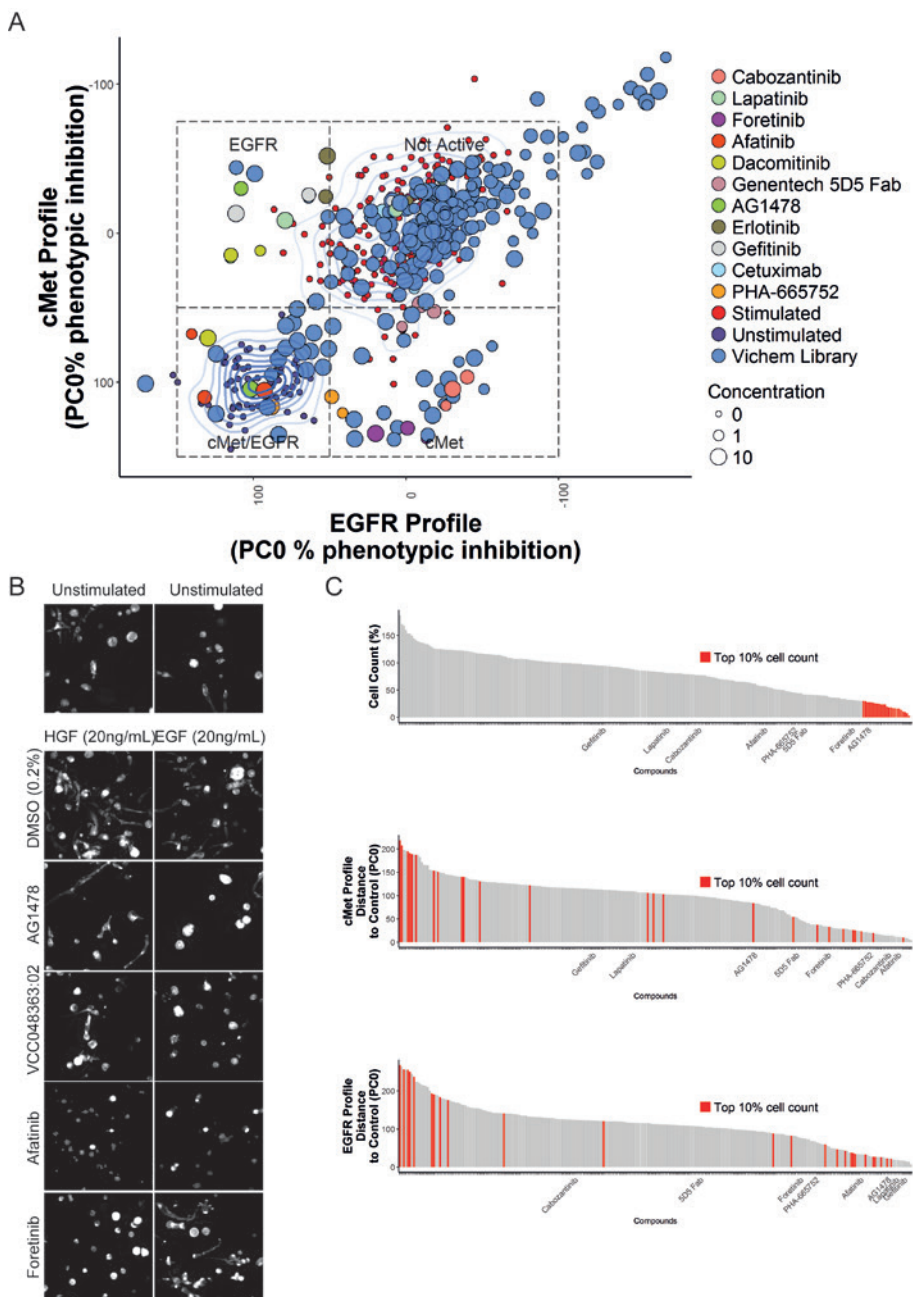


FIGURE 4 Identification of selective c-Met/EGFR inhibitors in a Vichem EGFR/c-Met inhibiting compound library. **A**) Compound screen of 80 Vichem compounds tested at 10, 3.16 and $1\mu\text{M}$. Compounds were divided over triplicate plates and co-exposed with either HGF (20ng/mL) or EGF (20ng/mL). PCA was trained on unstimulated and stimulated controls separately for plates exposed to HGF or EGF, respectively, to obtain (legend continues on next page)

a principal component that could separate c-Met and EGFR responses. Data points represent mean determinations from 3 wells. Controls are color-coded as indicated in the legend. For stimulated (top middle) and unstimulated controls (bottom left), a 2D-density estimation (contour lines) is shown. **B)** Representative 2D projected images derived from the F-actin staining after 96 hours of compound treatment. Except for AG1478, which was 3.16 μM , shown treatment concentrations were 10 μM . Pictures were obtained using a BD Pathway 855 microscope (images trimmed to 300x300 pixels for presentation purposes). **C)** Cell count (viability) is a poor criterion for selecting c-Met and EGFR inhibitors. Number of nuclei per well was %-normalized to stimulated control (100%) and lowest detected cell count and 0%, top panel. The top ranking 10% of compounds affecting cell count are colour-coded in red. Middle and lower panel shows the same compounds ranked on efficacy on c-Met and EGFR profiles (distance to unstimulated control). Mean values shown; each chart contains compounds at three different concentrations.

Using phenotype to discriminate compounds based on target selectivity.

To determine whether the phenotypic assay can discriminate between selective c-Met and EGF inhibitors, PC-3 cells were cultured in the presence of either HGF or EGF, together with established small molecule and antibody inhibitors of their cognate receptors. As expected, the small molecule c-Met inhibitor PHA-665752²²⁻²³ selectively inhibited the phenotype induced by HGF. In contrast, the EGFR inhibitor AG1478²⁴ had no significant effect on the HGF-induced phenotype up to a concentration of 1 μM (figure 3A and 3C, right panel). Conversely, AG1478 but not PHA-665752 inhibited the EGF-induced phenotype (figure 3A and 3C, left panel). These findings suggest that residual c-Met and EGFR activity does not contribute to the 3D phenotype under the conditions used and that c-Met does not require EGFR for the ligand induced response and vice versa. Interestingly, ArQ-197, which is reported to be a selective inhibitor of c-Met,²⁵⁻²⁶ inhibited both the HGF and EGF-induced responses with a similar IC_{50} , suggesting a more complex mechanism of action. At higher concentrations (>1 μM), this compound introduced a novel phenotype, shown by a shift away from the controls in a representation of phenotypic space (figure 3B).

To confirm that the interpretations based on phenotypic changes correlated with inhibition of receptor kinase activity, we performed Western blot analysis for phosphorylated c-Met (Y1234/-5) and phosphorylated EGFR (Y1173) (figure 3D). Results showed that PHA-665752 and the Genentech 5D5 Fab potentially inhibited phosphorylation of c-Met, but not EGFR phosphorylation. Conversely, AG1478 and cetuximab treatment inhibited phosphorylation of EGFR, but not of c-Met. ArQ-197 did not show detectable inhibition of EGFR (Y1173) or c-Met (Y1234/-5) phosphorylation under these conditions (figure 3D). Therefore, inhibition of phenotypes in 3D culture by c-Met and EGFR inhibitors correlates with inhibition of the respective kinases.

TABLE 1 Hit selection phenotypic screen

Vichem Compound-ID	1 μ M	3.16 μ M	10 μ M
VCC030450:22	EGFR	EGFR	EGFR
VCC048363:02	EGFR	EGFR	EGFR/cMet
VCC055393:01	EGFR/cMet	EGFR/cMet	EGFR/cMet
VCC109756:01	cMet	cMet	cMet
VCC155409:01	None	None	EGFR/cMet
VCC228833:01	None	None	Top 10% cell count
VCC285946:01	None	cMet	cMet
VCC376189:01	cMet	cMet	EGFR/cMet
VCC378728:01	None	EGFR	None
VCC407451:10	None	EGFR	EGFR
VCC415997:02	cMet	cMet	cMet
VCC429285:02	None	None	EGFR/cMet
VCC444414:01	cMet	cMet	cMet
VCC450892:17	cMet	cMet	cMet
VCC497510:01	cMet	cMet	EGFR/cMet
VCC502987:01	None	None	EGFR/cMet
VCC528301:01	None	None	EGFR/cMet
VCC656576:02	None	None	None
VCC716837:01	None	None	Top 10% cell count
VCC740005:11	None	EGFR	EGFR
VCC744093:03	None	None	None
VCC833029:24	None	None	EGFR
VCC868449:01	None	None	EGFR/cMet
VCC960450:01	cMet	cMet	cMet

TABLE 2 Enzyme activity measurement (percent inhibition)

Vichem Compound-ID	EGFR	EGFR	EGFR	c-Met	c-Met	c-Met
	Inh (%) 10 μ M	Inh (%) 1 μ M	Inh (%) 0.1 μ M	Inh (%) 10 μ M	Inh (%) 1 μ M	Inh (%) 0.1 μ M
VCC030450:22	101	99	97	4	2	0
VCC048363:02	101	100	97	1	-2	-1
VCC055393:01	99	100	100	3	3	-4
VCC109756:01	43	7	2	93	61	7
VCC155409:01	76	34	10	25	2	-2
VCC228833:01	16	1	0	4	0	-2
VCC285946:01	32	0	9	84	49	8
VCC376189:01	12	2	-2	83	56	9
VCC378728:01	85	41	8	72	16	0
VCC407451:10	93	92	73	7	0	-4
VCC415997:02	-11	-11	-7	95	77	14
VCC429285:02	3	2	0	6	-2	2
VCC444414:01	7	-4	-6	90	47	3
VCC450892:17	32	10	5	85	39	4
VCC497510:01	20	10	2	90	54	9
VCC502987:01	19	9	1	4	1	0
VCC528301:01	94	82	29	37	7	1
VCC656576:02	-2	-7	-13	0	-4	-4
VCC716837:01	48	10	1	41	6	0
VCC740005:11	105	102	93	11	1	3
VCC744093:03	77	25	3	27	-1	-1
VCC833029:24	97	90	37	-3	0	0
VCC868449:01	95	89	37	56	14	3
VCC960450:01	-11	-7	-10	87	50	11

Taken together, these results show that measurement of ligand-induced phenotypic changes can be used to discriminate and measure inhibition of c-Met and EGFR.

Using phenotypic profiles to identify novel selective c-Met and EGFR inhibitors

Using data obtained from c-Met and EGFR in vitro kinase assays, a collection of 80 putative single and dual specificity EGFR and c-Met inhibitors was compiled (supplemental table 1), which included several well-characterized reference compounds. These were screened in 3D-cultured PC-3 cells together with several published reference inhibitors of c-Met and EGFR. All compounds were screened in 384-well plates at three concentrations (10 μ M, 3.16 μ M and 1 μ M) in triplicate plates in both EGF- and HGF-stimulated conditions. Multiparametric analysis was performed as before, followed by Z-score normalisation of each parameter to the plate median. Supervised principal components analysis was used to condense phenotypic measurements to one phenotypic descriptor (PCo), which was scaled to %-inhibition. PCA was found to perform superior to individual features in separating out stimulated and unstimulated controls (supplemental figure 2).

Figure 4A depicts the screening results combining the first principal component, PCo, for both EGF- and HGF-induced phenotypic changes in a single plot. Inhibition of c-Met is therefore represented by a decrease in the c-Met PCo value, from the growth factor-treated to growth factor-untreated controls. Compounds that induced such a shift in the c-Met PCo included various established c-Met reference inhibitors that were included in the screen, including the Genentech 5D5 Fab antibody, foretinib and lower doses of PHA-665752. This confirmed that the phenotypic training using HGF treated and untreated samples discriminated c-Met active and inactive conditions and was able to select compounds that induced a c-Met inhibitory phenotypic profile. Selective inhibition of the EGFR could be characterized by a horizontal shift to the left, from a profile associated with EGF-stimulated phenotype to one associated with an unstimulated phenotype. This region contained several EGFR reference inhibitors, including erlotinib, gefitinib and AG1478 (at 1 and 3.16 μ M), which were included in the screen alongside test compounds. Compounds that clustered together with the unstimulated controls (figure 4A, bottom left quadrant) were predicted to have a dual inhibitory activity for both c-Met and EGFR. The compounds clustering in this area included afatinib, and also a number of previously untested compounds of the Vichem library. The class to which each compound was attributed using this approach is shown in table 1 and supplemental table 2. By using another form of supervised clustering, linear discriminant analysis (LDA), we could separate the highly similar EGF- and HGF-induced phenotypes into a multidimensional plot (supplemental figure 3). However, this approach did not improve classification of reference c-Met and EGFR inhibitor compounds.

Representative images of 3D-cultured PC-3 cells treated with EGFR and c-Met inhibitors are presented in figure 4B and show a consistency between the automated classification of compounds to a specific inhibitory class and the phenotype which is induced in the presence of a specific growth factor. We compared the pheno-

typic classification of compounds with measurements of EGFR or c-Met enzyme inhibitory activity (table 2 and supplemental table 3). Phenotypic classification was found to frequently overlap with biochemical measurements. Inhibition of c-Met activity in enzymatic and phenotypic assays was closely correlated, with all compounds showing greater than 40% inhibition in an enzymatic assay being inhibitory in the phenotypic assay at the equivalent concentration. However, approximately half of the compounds that were active in EGFR enzymatic assays were inactive in the cell based phenotypic assays. Furthermore, several of the compounds that were inhibitory at the lowest doses in the EGFR enzymatic assay, only showed activity in the corresponding phenotypic assay at higher concentrations (e.g. VCC833029:24, VCC740005:11 and VCC407451:10), indicating lower sensitivity of the phenotypic assay compared to the enzymatic assay. Not all compounds that induced enzymatic inhibition of EGFR and/or c-Met could be identified as inhibitors from our screening results, suggesting that enzymatic inhibition does not directly translate to a phenotypic change under all conditions.

We then compared ranking of compounds based on phenotypic profiling with ranking based on cell count. Cell count was determined by the number of nuclei counted per well (one of the many features scored by the multiparametric analysis) and is a feature that correlates closely with biochemical measurements of cell proliferation (not shown). Using a ranking based on cell proliferation, inhibitors which were shown to potently inhibit the c-Met phenotype, including Genentech 5D5 Fab, did not score in the top 10% inhibitors of proliferation (Figure 4C and supplemental figure 4). Consistent with the profiling results in figure 4A, when compounds were ranked based on the difference of their phenotypic profiles to unstimulated controls (measured along PCo), a strong enrichment of c-Met and EGFR inhibitors was observed in the top 10% of ranked compounds in the presence of HGF and EGF respectively (supplemental figure 4). The most potent inhibitors of proliferation were found to perform poorly when ranked based on their phenotypic profiles (figure 4C). An analysis of the images from 3D cultures treated with these compounds showed that spheroid formation was disrupted, consistent with cytotoxicity of these compounds.

Discussion

Because tumour cells exist in a 3D extracellular matrix-rich environment, 3D matrix-embedded cell cultures provide a more physiologically relevant context in which to perform compound screening.²⁻⁴ The increased complexity of 3D cultures also offers increased potential for phenotypic profiling.²⁷⁻²⁹ We developed a fully scalable 3D tissue culture-based high-content screening platform that uses phenotypic profiling of cultured tumouroids derived from a prostate cancer cell line. This screening platform was used to identify several selective inhibitors for c-Met and EGFR, which represent important targets in many cancers and are known to be able to stimulate survival and invasive growth of tumours.¹⁵⁻¹⁷ We show that activation of c-Met with its ligand, HGF, induced a dose-dependent reorganisation of PC-3 spheroids characterized by invasion of cells into the surrounding matrix. A similar change in phenotype was induced by the addition of EGF to the PC-3 cells. These phenotypic changes were not observed in 2D

monolayers. Ultra-high content multiparametric analysis allowed a clear discrimination of the phenotypes associated with active and inactive c-Met and EGFR, which could be quantified using a single PCA measurement. This approach allowed us to discriminate inhibitors of c-Met and EGFR and also putative bi-selective inhibitors of these receptor tyrosine kinases. The method also enabled non-selective compounds to be discriminated since they induced phenotypes that failed to match those induced by selective inhibition of c-Met or EGFR. The screening results were cross-validated with an *in vitro* measurement of enzyme activity, and were found to largely correlate. Some compounds that inhibited EGFR or c-Met in the biochemical measurement were not identified by our phenotypic screen as inhibitors for these pathways, indicating that inhibition of purified enzyme does not always correlate with inhibition of the target enzyme in cells. These differences may be explained by poor compound stability over multiple days in aqueous solution (medium) or poor membrane permeability, resulting in lower cytoplasmic concentrations. It is also possible that these compounds induce mild phenotypic changes that are below the threshold of the phenotypic assay. A number of compounds were found to induce phenotypic changes in the EGFR and/or c-Met profiles, even though these failed to induce inhibition of either EGFR or c-Met activity. A possible explanation for this finding is that these molecules induced off-target phenotypic effects that could not be discriminated from inhibition of c-Met and EGFR.

Improvements in 3D cell culture reagents, methods and automated microscopes that can capture 3D image data is making screening in 3D more accessible, including more complex models such as co-cultures.^{5, 30} Here we describe how high content analysis can maximise the information that can be extracted from the more complex phenotypes obtained in 3D cell culture. These include disease-relevant features, such as tumour cell invasion, but also a multitude of other features that can be exploited for profiling purposes. Thus, in addition to screening for inhibition of a disease phenotype, target based screening can be performed. Traditionally, receptor activation has been measured using biochemical methods. While sensitive, these methods do not discriminate non-selective inhibition of the target. An advantage of the multiparametric profiling approach described here is that in addition to detecting inhibition of the c-Met and EGFR, off-target effects can also be detected if the off-targets have an impact on tissue phenotype.

Our method was used to determine inhibitory activity of both small molecules and antibodies. We applied the method to both c-Met and EGFR but, in principle, it can be applied to any target if a cell line can be identified in which the activity of the target influences cell phenotype. Combining the advantages of physiological relevance and phenotypic complexity, phenotypic screening and profiling with 3D cell cultures has the potential to improve the quality of hits from screens and make previously challenging targets more accessible, potentially leading to a higher success rate of molecules in clinical trials.

Acknowledgments

The authors would like to thank Souichi Ogata (Janssen Oncology R&D) for kindly providing ArQ-197 and Rob Roovers (Merus) for providing the Genentech 5D5 Fab and IgG. Furthermore, we thank Dr Marc Bickle, Max Planck, Dresden, for introducing us to the KNIME software.

References

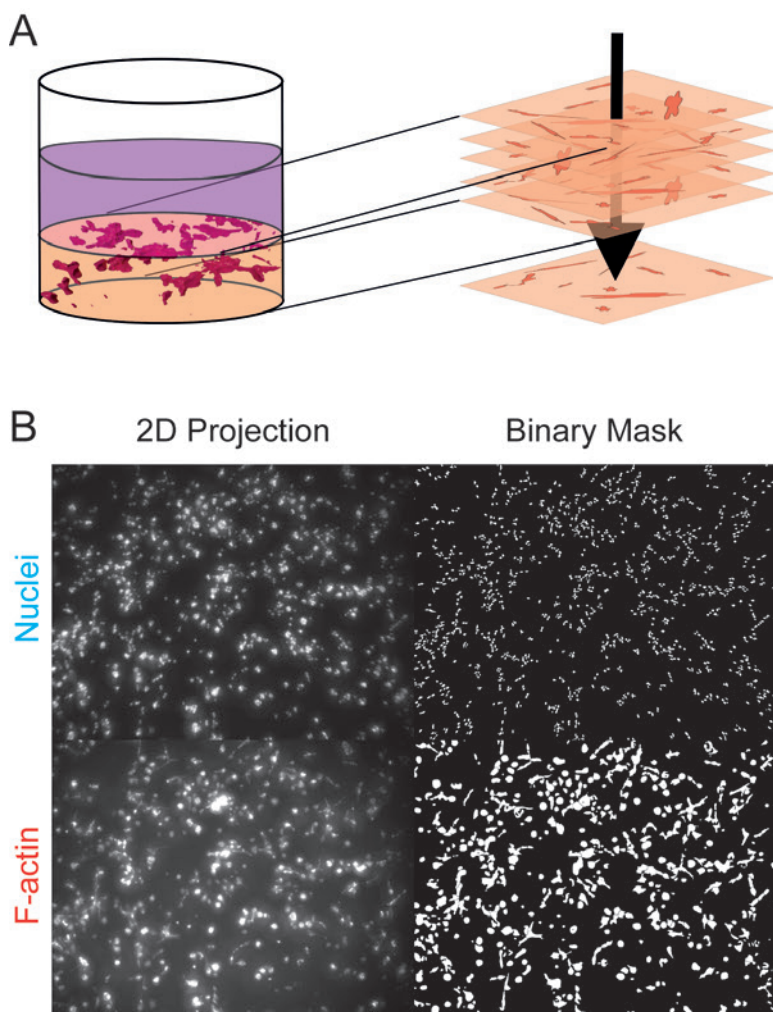
1. Mishra DK, Sakamoto JH, Thrall MJ, Baird BN, Blackmon SH, Ferrari M, Kurie JM, Kim MP: Human lung cancer cells grown in an ex vivo 3D lung model produce matrix metalloproteinases not produced in 2D culture. *PLoS One* 7(9): e45308, 2012
2. Bradbury P, Fabry B, O'Neill GM: Occupy tissue: the movement in cancer metastasis. *Cell Adh Migr* 6(5): 424-432, 2012
3. Smalley KS, Lioni M, Herlyn M: Life isn't flat: taking cancer biology to the next dimension. *In Vitro Cell Dev Biol Anim* 42(8-9): 242-247, 2006
4. Breslin S, O'Driscoll L: Three-dimensional cell culture: the missing link in drug discovery. *Drug Discov Today* 18(5-6): 240-249, 2013
5. Li L, Zhou Q, Voss TC, Quick KL, LaBarbera DV: High-throughput imaging: Focusing in on drug discovery in 3D. *Methods* 96 97-102, 2016
6. Taubenberger AV, Bray LJ, Haller B, Shaposhnykov A, Binner M, Freudenberg U, Guck J, Werner C: 3D extracellular matrix interactions modulate tumour cell growth, invasion and angiogenesis in engineered tumour microenvironments. *Acta Biomater* 36 73-85, 2016
7. Debnath J, Brugge JS: Modelling glandular epithelial cancers in three-dimensional cultures. *Nat Rev Cancer* 5(9): 675-688, 2005
8. Schmeichel KL, Bissell MJ: Modeling tissue-specific signaling and organ function in three dimensions. *J Cell Sci* 116(Pt 12): 2377-2388, 2003
9. O'Brien LE, Zegers MM, Mostov KE: Opinion: Building epithelial architecture: insights from three-dimensional culture models. *Nat Rev Mol Cell Biol* 3(7): 531-537, 2002
10. Harma V, Knuutila M, Virtanen J, Mirtti T, Kohonen P, Kovanen P, Happonen A, Kaewphan S, Ahonen I, Kallioniemi O, Grafstrom R, Lotjonen J, Nees M: Lysophosphatidic acid and sphingosine-1-phosphate promote morphogenesis and block invasion of prostate cancer cells in three-dimensional organotypic models. *Oncogene* 31(16): 2075-2089, 2012
11. Ren Y, Cao B, Law S, Xie Y, Lee PY, Cheung L, Chen Y, Huang X, Chan HM, Zhao P, Luk J, Vande Woude G, Wong J: Hepatocyte growth factor promotes cancer cell migration and angiogenic factors expression: a prognostic marker of human esophageal squamous cell carcinomas. *Clin Cancer Res* 11(17): 6190-6197, 2005
12. Chan GK, Lutterbach BA, Pan BS, Kariv I, Szewczak AA: High-throughput analysis of HGF-stimulated cell scattering. *J Biomol Screen* 13(9): 847-854, 2008
13. Radtke S, Milanovic M, Rosse C, De Rycker M, Lachmann S, Hibbert A, Kermorgant S, Parker PJ: ERK2 but not ERK1 mediates HGF-induced motility in non-small cell lung carcinoma cell lines. *J Cell Sci* 126(Pt 11): 2381-2391, 2013

14. Zaritsky A, Natan S, Ben-Jacob E, Tsarfaty I: Emergence of HGF/SF-induced coordinated cellular motility. *PLoS One* 7(9): e44671, 2012
15. Comoglio PM, Trusolino L: Invasive growth: from development to metastasis. *J Clin Invest* 109(7): 857-862, 2002
16. Hardy KM, Booth BW, Hendrix MJ, Salomon DS, Strizzi L: ErbB/EGF signaling and EMT in mammary development and breast cancer. *J Mammary Gland Biol Neoplasia* 15(2): 191-199, 2010
17. Appert-Collin A, Hubert P, Cremel G, Bennisroune A: Role of ErbB Receptors in Cancer Cell Migration and Invasion. *Front Pharmacol* 6 283, 2015
18. Di Z, Klop MJ, Rogkoti VM, Le Devedec SE, van de Water B, Verbeek FJ, Price LS, Meerman JH: Ultra high content image analysis and phenotype profiling of 3D cultured micro-tissues. *PLoS One* 9(10): e109688, 2014
19. Venables WNR, B.D.: Modern Applied Statistics with S. In: edited by Springer-Verlag New York, 2002,
20. Wickham H: ggplot2: Elegant Graphics for Data Analysis. In: edited by Springer Publishing Company, Incorporated, 2009,
21. Ligges UM, M.: Scatterplot3d - An R Package for Visualizing Multivariate Data. *Journal of Statistical Software* 008(i11): 20, 2003
22. Tu WH, Zhu C, Clark C, Christensen JG, Sun Z: Efficacy of c-Met inhibitor for advanced prostate cancer. *BMC Cancer* 10 556, 2010
23. Yang Y, Wislez M, Fujimoto N, Prudkin L, Izzo JG, Uno F, Ji L, Hanna AE, Langley RR, Liu D, Johnson FM, Wistuba I, Kurie JM: A selective small molecule inhibitor of c-Met, PHA-665752, reverses lung premalignancy induced by mutant K-ras. *Mol Cancer Ther* 7(4): 952-960, 2008
24. Caja L, Sancho P, Bertran E, Ortiz C, Campbell JS, Fausto N, Fabregat I: The tyrphostin AG1478 inhibits proliferation and induces death of liver tumor cells through EGF receptor-dependent and independent mechanisms. *Biochem Pharmacol* 82(11): 1583-1592, 2011
25. Adjei AA, Schwartz B, Garmey E: Early clinical development of ARQ 197, a selective, non-ATP-competitive inhibitor targeting MET tyrosine kinase for the treatment of advanced cancers. *Oncologist* 16(6): 788-799, 2011
26. Feldman DR, Einhorn LH, Quinn DI, Loriot Y, Joffe JK, Vaughn DJ, Flechon A, Hajdenberg J, Halim AB, Zahir H, Motzer RJ: A phase 2 multicenter study of tivantinib (ARQ 197) monotherapy in patients with relapsed or refractory germ cell tumors. *Invest New Drugs* 31(4): 1016-1022, 2013
27. Sirenko O, Mitlo T, Hesley J, Luke S, Owens W, Cromwell EF: High-content assays for characterizing the viability and morphology of 3D cancer spheroid cultures. *Assay Drug Dev Technol* 13(7): 402-414, 2015
28. Harma V, Schukov HP, Happonen A, Ahonen I, Virtanen J, Siitari H, Akerfelt M, Lotjonen J, Nees M: Quantification of dynamic morphological drug responses in 3D organotypic cell cultures by automated image analysis. *PLoS One* 9(5): e96426, 2014

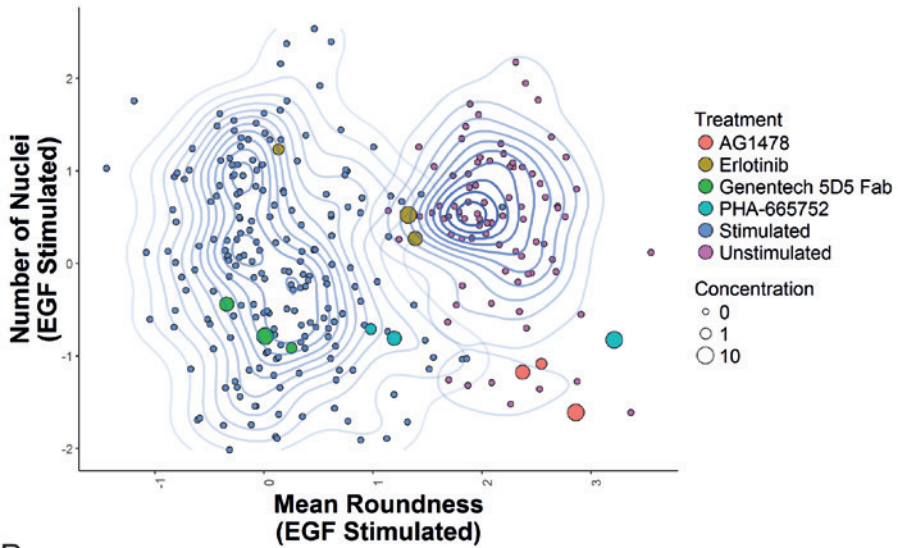
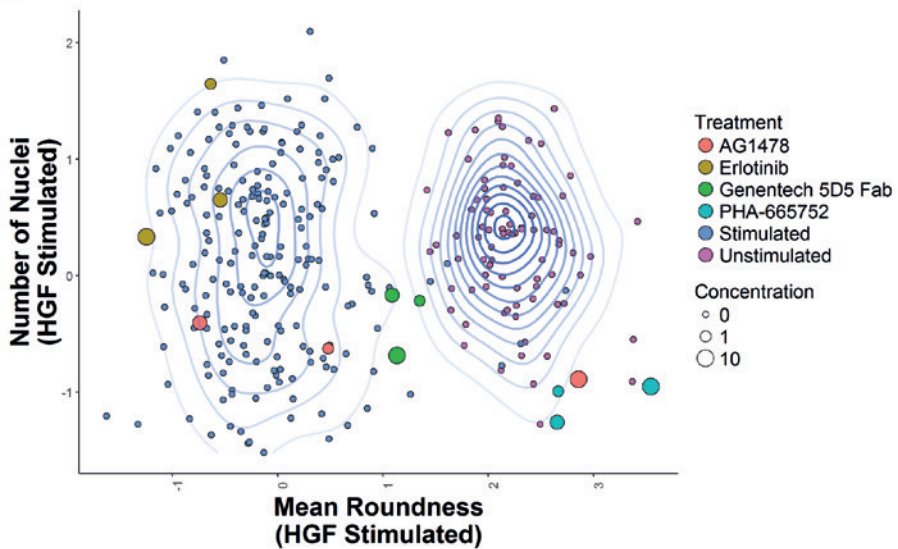
29. Robinson S, Guyon L, Nevalainen J, Toriseva M, Akerfelt M, Nees M: Segmentation of Image Data from Complex Organotypic 3D Models of Cancer Tissues with Markov Random Fields. *PLoS One* 10(12): e0143798, 2015
30. Krausz E, de Hoogt R, Gustin E, Cornelissen F, Grand-Perret T, Janssen L, Vloemans N, Wuyts D, Frans S, Axel A, Peeters PJ, Hall B, Cik M: Translation of a tumor microenvironment mimicking 3D tumor growth co-culture assay platform to high-content screening. *J Biomol Screen* 18(1): 54-66, 2013

SUPPLEMENTAL MATERIALS

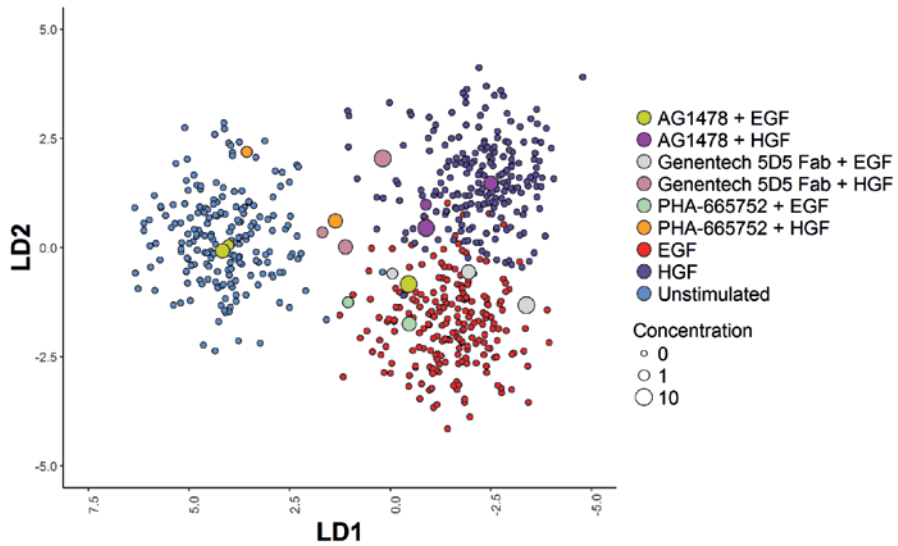
3



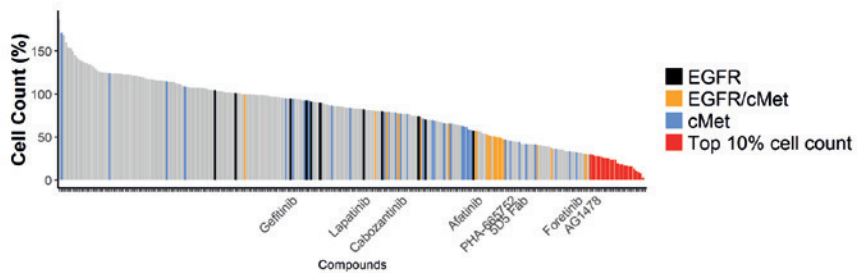
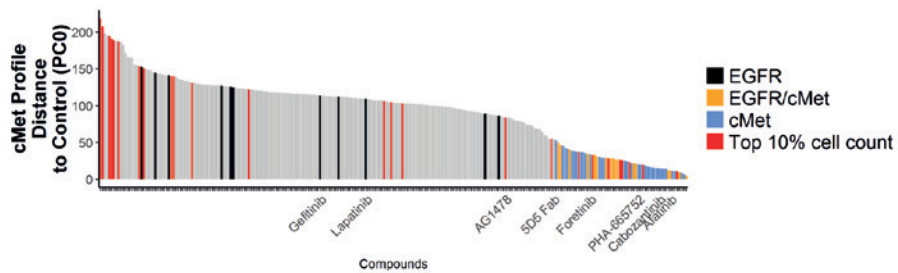
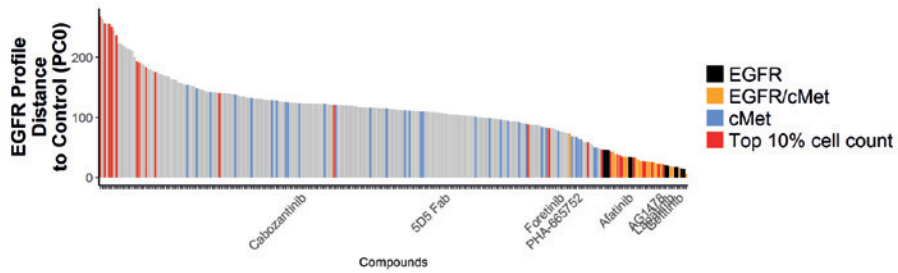
SUPPLEMENTAL FIGURE 1 3D cell culture based screening platform pipeline. **A)** PC-3 cells were cultured in 384 well plate format embedded in ECM-protein hydrogels. Compound treatment was performed for 96 hours, after which the 3D cultures were stained for F-actin and nuclei. Images were obtained for both channels at different z-planes in the gel using a BD Pathway 855 imager. In-focus information of all Z-stacks was extracted by means of a 2D maximum intensity projection. **B)** Binary black and white masks were generated to define the segmented objects and were used for shape measurements. Fluorescence intensity parameters were obtained from the segmented regions of the original micrograph projection.

A**B**

SUPPLEMENTAL FIGURE 2 Performance of individual phenotypic parameters to identify selective c-Met or EGFR inhibitors. **A)** Z-score normalized roundness and number of nuclei of tumouroids shown for EGF stimulated condition. **B)** Z-score normalized roundness and number of nuclei of tumouroids shown for HGF stimulated condition.



SUPPLEMENTAL FIGURE 3 EGF-and HGF-induced phenotypes are both characterized by invasion into the ECM, but can be differentiated using linear discriminant analysis (LDA). LDA training was performed using KNIME and RStudio (MASS package). Linear correlation filter was applied to all parameters ($R^2 < 0.85$) prior to training LDA on EGF, HGF and unstimulated groups, in order to filter out the most highly collinear variables. Approximately 250 phenotypic descriptors are required to separate both phenotypes. LDA was subsequently applied to the complete dataset. Individual data points for EGF, HGF and unstimulated shown. Mean data shown for AG1478, Genentech 5D5 Fab and PHA-665752.



SUPPLEMENTAL FIGURE 4 Hit selection based on cell count does not identify selective c-Met and EGFR inhibitors. Ranking performed on cell count and on c-Met and EGFR profile, as in figure 4C, show different results.

SUPPLEMENTAL TABLE 1 Vichem compound information

3

Compound ID	References	Core structure
VCC030450:22	D.W.Fry et al. 1994 Science 265, 1093-95.	quinazoline
VCC613596:10	WO 2009104027 A1	benzothienio[2,3-d]pyrimidine
VCC912492:07	WO 2012080727 A2	benzothienio[2,3-d]pyrimidine
VCC740005:11	Cancer Res, Vol.65 Nr., 379-382, 2005.	quinazoline
VCC407451:10	Bioorg Med Chem Lett, Vol.14 Nr.1, 111-114, 2004.	quinazoline
VCC075648:03	J. Med. Chem., 1999, 42, 5120-5130, Cancer Research (2003), 63(17), 5462-5469	indol-2-one
VCC475979:01	unpublished	indol-2-one
VCC884444:01	unpublished	indol-2-one
VCC833029:24	Bioorg Med Chem Lett, Vol.16 Nr.17, 4686-4691, 2006.	quinazoline
VCC502987:01	unpublished	indol-2-one
VCC370686:02	unpublished	indol-2-one
VCC703724:02	unpublished	indol-2-one
VCC260084:01	unpublished	indol-2-one
VCC458127:03	Bioorg. Med. Chem.Lett. 2001,11,2867-2870	4-(1H-imidazol-5-yl)pyrimidine
VCC930986:01	Tetrahedron Letters (2008), 49(7), 1269-1273.	quinazoline
VCC996608:06	Current Medicinal Chemistry (2014), 21(17), 1938-1955.	quinoline
VCC398520:05	Preparation of quinoline derivatives as AXL kinase inhibitors WO 2009127417 A1	quinoline
VCC285946:01	Molecular Cancer Therapeutics (2009), 8(12), 3181-3190.	[1,2,4]triazolo[4,3-b]pyridazine
VCC055393:01	2008 Oncogene 27 (34), pp. 4702-4711	quinazoline
VCC131028:02	unpublished	quinoline
VCC098211:02	unpublished	quinoline
VCC999628:01	unpublished	quinoline
VCC376189:01	ACS Medicinal Chemistry Letters (2014), 5(4), 298-303.	quinoline
VCC967844:01	ACS Medicinal Chemistry Letters (2014), 5(4), 298-303.	quinoline
VCC617235:01	unpublished	quinoline
VCC395122:01	ACS Medicinal Chemistry Letters (2014), 5(4), 298-303.	quinoline
VCC883733:01	ACS Medicinal Chemistry Letters (2014), 5(4), 298-303.	quinoline
VCC868449:01	ACS Medicinal Chemistry Letters (2014), 5(4), 298-303.	quinoline
VCC155409:01	ACS Medicinal Chemistry Letters (2014), 5(4), 298-303.	quinoline
VCC048363:02	Clinical Cancer Research 2009, 15, 5040, Cancer Res 2007;67(24):11924-32	quinazoline
VCC957400:02	ACS Medicinal Chemistry Letters (2014), 5(4), 298-303.	quinoline
VCC716837:01	ACS Medicinal Chemistry Letters (2014), 5(4), 298-303.	quinoline
VCC656237:01	unpublished	quinoline
VCC378728:01	ACS Medicinal Chemistry Letters (2014), 5(4), 298-303.	quinoline
VCC461663:01	unpublished	quinoline
VCC325112:01	ACS Medicinal Chemistry Letters (2014), 5(4), 298-303.	quinoline
VCC109756:01	ACS Medicinal Chemistry Letters (2014), 5(4), 298-303	quinoline
VCC497510:01	ACS Medicinal Chemistry Letters (2014), 5(4), 298-303.	quinoline
VCC444414:01	ACS Medicinal Chemistry Letters (2014), 5(4), 298-303.	quinoline
VCC960450:01	Clin Cancer Res. 2010 Dec 15;16(24):5936-41.	quinoline
VCC450892:17	Cancer Res. 2009 Oct 15;69(20):8009-16.	quinoline
VCC528301:01	ACS Medicinal Chemistry Letters (2014), 5(4), 298-303.	quinoline
VCC778672:01	ACS Medicinal Chemistry Letters (2014), 5(4), 298-303.	quinoline
VCC466812:01	ACS Medicinal Chemistry Letters (2014), 5(4), 298-303.	quinoline
VCC444508:05	ACS Medicinal Chemistry Letters (2014), 5(4), 298-303.	quinoline
VCC590177:01	unpublished	quinoline
VCC221701:01	Preparation of benzopyrrolidone derivatives for use as GRK5 modulators WO 2015022437 A1	indol-2-one
VCC979277:01	Preparation of benzopyrrolidone derivatives for use as GRK5 modulators WO 2015022437 A1	indol-2-one

(table continues on next page)

VCC935482:01	Preparation of benzopyrrolidone derivatives for use as GRK5 modulators 2015022437 A1	WO	indol-2-one
VCC443915:01	Preparation of benzopyrrolidone derivatives for use as GRK5 modulators 2015022437 A1	WO	indol-2-one
VCC051013:02	Preparation of benzopyrrolidone derivatives for use as GRK5 modulators 2015022437 A1	WO	indol-2-one
VCC228833:01	Preparation of benzopyrrolidone derivatives for use as GRK5 modulators 2015022437 A1	WO	indol-2-one
VCC685240:01	Preparation of benzopyrrolidone derivatives for use as GRK5 modulators 2015022437 A1	WO	indol-2-one
VCC804481:01	Preparation of benzopyrrolidone derivatives for use as GRK5 modulators 2015022437 A1	WO	indol-2-one
VCC365775:01	Preparation of benzopyrrolidone derivatives for use as GRK5 modulators 2015022437 A1	WO	indol-2-one
VCC744093:03	Preparation of benzopyrrolidone derivatives for use as GRK5 modulators 2015022437 A1	WO	indol-2-one
VCC323972:01	WO 2014022116 A2 20140206		4-phenoxyppyridine
VCC353749:01	Preparation of benzopyrrolidone derivatives for use as GRK5 modulators 2015022437 A1	WO	indol-2-one
VCC317779:01	WO 2014022116 A2 20140206		4-phenoxyppyridine
VCC415997:02	WO 2008102870 A1		4-phenoxyppyridine
VCC055876:02	Preparation of benzopyrrolidone derivatives for use as GRK5 modulators 2015022437 A1	WO	4-phenoxyppyridine
VCC429285:02	Preparation of benzopyrrolidone derivatives for use as GRK5 modulators 2015022437 A1	WO	indol-2-one
VCC372550:01	Preparation of benzopyrrolidone derivatives for use as GRK5 modulators 2015022437 A1	WO	indol-2-one
VCC290183:01	Preparation of benzopyrrolidone derivatives for use as GRK5 modulators 2015022437 A1	WO	indol-2-one
VCC031393:01	Preparation of benzopyrrolidone derivatives for use as GRK5 modulators 2015022437 A1	WO	indol-2-one
VCC346202:02	Preparation of benzopyrrolidone derivatives for use as GRK5 modulators 2015022437 A1	WO	indol-2-one
VCC563740:02	Preparation of benzopyrrolidone derivatives for use as GRK5 modulators 2015022437 A1	WO	indol-2-one
VCC180368:02	unpublished		quinoline
VCC239215:01	unpublished		4-phenoxyppyridine
VCC898902:01	unpublished		4-phenoxyppyridine
VCC733981:01	unpublished		4-phenoxyppyridine
VCC656576:02	unpublished		4-phenoxyppyridine
VCC034014:01	unpublished		4-phenoxyppyridine
VCC132459:01	unpublished		4-phenoxyppyridine
VCC692601:01	unpublished		4-phenoxyppyridine
VCC581800:03	unpublished		quinoline
VCC232089:02	Preparation of benzopyrrolidone derivatives for use as GRK5 modulators 2015022437 A1	WO	indol-2-one
VCC650454:03	Preparation of benzopyrrolidone derivatives for use as GRK5 modulators 2015022437 A1	WO	indol-2-one
VCC227946:01	Preparation of benzopyrrolidone derivatives for use as GRK5 modulators 2015022437 A1	WO	indol-2-one

SUPPLEMENTAL TABLE 2 Hit selection phenotypic screen

3

Vicium ID	1µM	3.16 µM	10 µM
VCC030450:22	EGFR	EGFR	EGFR
VCC031393:01	Top 10% cell count	None	cMet
VCC034014:01	None	None	None
VCC048363:02	EGFR	EGFR	EGFR/cMet
VCC051013:02	Top 10% cell count	Top 10% cell count	None
VCC055393:01	EGFR/cMet	EGFR/cMet	EGFR/cMet
VCC055876:02	None	None	None
VCC075648:03	None	None	None
VCC098211:02	None	None	None
VCC109756:01	cMet	cMet	cMet
VCC131028:02	None	None	None
VCC132459:01	None	None	None
VCC155409:01	None	None	EGFR/cMet
VCC180368:02	None	None	None
VCC221701:01	None	None	None
VCC227946:01	None	None	EGFR/cMet
VCC228833:01	None	None	Top 10% cell count
VCC232089:02	None	None	Top 10% cell count
VCC239215:01	None	None	None
VCC260084:01	None	None	None
VCC285946:01	None	cMet	cMet
VCC290183:01	None	None	None
VCC317779:01	None	None	None
VCC323972:01	None	None	None
VCC325112:01	None	None	None
VCC346202:02	Top 10% cell count	Top 10% cell count	Top 10% cell count
VCC353749:01	None	None	None
VCC365775:01	None	None	cMet
VCC370686:02	None	None	None
VCC372550:01	None	None	None
VCC376189:01	cMet	cMet	EGFR/cMet
VCC378728:01	None	EGFR	None
VCC395122:01	None	None	cMet
VCC398520:05	None	None	None
VCC407451:10	None	EGFR	EGFR
VCC415997:02	cMet	cMet	cMet
VCC429285:02	None	None	EGFR/cMet
VCC443915:01	Top 10% cell count	None	cMet
VCC444414:01	cMet	cMet	cMet
VCC444508:05	None	None	Top 10% cell count
VCC450892:17	cMet	cMet	cMet
VCC458127:03	None	None	EGFR/cMet
VCC461663:01	None	None	None
VCC466812:01	None	None	None
VCC475979:01	None	None	Top 10% cell count
VCC497510:01	cMet	cMet	EGFR/cMet
VCC502987:01	None	None	EGFR/cMet
VCC528301:01	None	None	EGFR/cMet
VCC563740:02	None	Top 10% cell count	None
VCC581800:03	cMet	cMet	cMet
VCC590177:01	None	None	None
VCC613596:10	None	None	None
VCC617235:01	None	None	None
VCC650454:03	Top 10% cell count	Top 10% cell count	Top 10% cell count
VCC656237:01	None	None	None
VCC656576:02	None	None	None
VCC685240:01	None	None	cMet
VCC692601:01	None	None	None
VCC703724:02	None	None	None
VCC716837:01	None	None	Top 10% cell count
VCC733981:01	None	None	None
VCC740005:11	None	EGFR	EGFR
VCC744093:01	None	None	None
VCC744093:03	None	Top 10% cell count	EGFR/cMet
VCC778672:01	None	None	None
VCC804481:01	None	None	Top 10% cell count
VCC833029:24	None	None	EGFR
VCC868449:01	None	None	EGFR/cMet
VCC883733:01	None	None	None
VCC884444:01	None	None	Top 10% cell count
VCC898902:01	None	None	None
VCC912492:07	None	None	None
VCC930986:01	None	None	None
VCC935482:01	None	None	None
VCC957400:02	None	None	Top 10% cell count
VCC960450:01	cMet	cMet	cMet
VCC967844:01	None	None	None
VCC979277:01	None	None	EGFR/cMet
VCC996608:06	None	None	Top 10% cell count
VCC99628:01	None	None	None

SUPPLEMENTAL TABLE 3 Enzyme activity measurement (% inhibition)

Vichem Compound-ID	EGFR Inh (%) 10µM	EGFR Inh (%) 1µM	EGFR Inh (%) 0.1µM	c-Met Inh (%) 10µM	c-Met Inh (%) 1µM	c-Met Inh (%) 0.1µM
VCC030450.22	101	99	97	4	2	0
VCC031393.01	11	2		16	0	
VCC034014.01	18	3		2	5	
VCC048363.02	101	100	97	1	-2	-1
VCC051013.02	16	0		41	6	
VCC055393.01	99	100	100	3	3	-4
VCC055876.02	-2	-9		22	-1	
VCC075648.03	66	13		41	6	
VCC098211.02	47	7		26	1	
VCC109756.01	43	7	2	93	61	7
VCC131028.02	30	-2		12	-4	
VCC132459.01	6	0		7	0	
VCC155409.01	76	34	10	25	2	-2
VCC180368.02	92	83		35	7	
VCC221701.01	22	4		22	1	
VCC227946.01	8					
VCC228833.01	16	1	0	4	0	-2
VCC232089.02	69					
VCC239215.01	17	4		16	4	
VCC260084.01	8	3		2	1	
VCC285946.01	32	0	9	84	49	8
VCC290183.01	16	4		27	3	
VCC317779.01	3	-1		82	18	
VCC323979.01	-2	-8		19	4	
VCC325112.01	59	16		44	4	
VCC346202.02	3	1		25	2	
VCC353749.01	5	1		26	1	
VCC365775.01	13	4		36	5	
VCC370686.02	-4	-8		2	-3	
VCC372550.01	-12	-9		2	-2	
VCC376189.01	12	2	-2	83	56	9
VCC378728.01	85	41	8	72	16	0
VCC395122.01	93	69	10	52	2	-3
VCC398520.05	98	55		87	30	
VCC407451.10	93	92	73	7	0	-4
VCC415997.02	-11	-11	-7	95	77	14
VCC429285.02	3	2	0	6	-2	2
VCC443915.01	23	3		27	1	
VCC44414.01	7	-4	-6	90	47	3
VCC444508.05	100	93		41	8	
VCC450892.17	32	10	5	85	39	4
VCC458127.03	95	62		3	0	
VCC461663.01	88	43		51	7	
VCC466812.01	102	84		67	13	
VCC475979.01	20	10		14	1	
VCC497510.01	20	10	2	90	54	9
VCC502987.01	19	9	1	4	1	0
VCC528301.01	94	82	29	37	7	1
VCC563740.02	15	10		25	5	
VCC581800.03	50			100		
VCC590177.01	94	67		56	3	
VCC613596.10	91	55		0	-1	
VCC617235.01	80	25		37	4	
VCC650454.03	39					
VCC656237.01	81	43		43	8	
VCC656576.02	-2	-7	-13	0	-4	-4
VCC685240.01	10	-6		4	1	
VCC692601.01	5	4		20	7	
VCC703724.02	9	9		7	4	
VCC716837.01	48	10	1	41	6	0
VCC733981.01	9	5		8	1	
VCC740005.11	105	102	93	11	1	3
VCC744093.03	77	25	3	27	-1	-1
VCC778672.01	101	85		56	9	
VCC804481.01	3	5		12	0	
VCC833029.24	97	90	37	-3	0	0
VCC868449.01	95	89	37	56	14	3
VCC883733.01	81	40		42	12	
VCC884444.01	2	-9		3	-2	
VCC898902.01	7	5		5	0	
VCC912492.07	87	47		2	-1	
VCC930986.01	92	49		0	-2	
VCC935482.01	-3	-2		-1	-3	
VCC957400.02	83	37		25	0	
VCC960450.01	-11	-7	-10	87	50	11
VCC967844.01	87	33		39	6	
VCC979277.01	12	5		17	3	
VCC996608.06	96	58		81	26	
VCC999628.01	26	0		14	1	

